Pediatric Radiology (2021) 51:1299–1310
https://doi.org/10.1007/s00247-021-05011-0

ORIGINAL ARTICLE

Accuracy of computed tomography angiography and structured reporting of high-risk morphology in anomalous aortic origin of coronary artery: comparison with surgery

Rajesh Krishnamurthy[1] · Prakash M. Masand[2] · Siddharth P. Jadhav[2] · Silvana Molossi[3] · Wei Zhang[4] · Hitesh M. Agrawal[5] · Carlos M. Mery[6]

Received: 7 August 2020 / Revised: 13 December 2020 / Accepted: 8 February 2021 / Published online: 23 March 2021

Abstract

Background Morphological features including interarterial course, intramural course, high ostial location and slit-like ostium are presumed risk factors for sudden cardiac death in children with anomalous aortic origin of the coronary artery (AAOCA). To facilitate clinical risk stratification, the diagnostic accuracy of CT angiography for individual risk factors in the setting of AAOCA must be established.

Objective We assessed diagnostic accuracy of standardized CT angiography interpretation for morphological characteristics that might determine risk in children with AAOCA by comparing them to surgical findings.

Materials and methods We created a standardized protocol for CT angiography of AAOCA and retrospectively evaluated diagnostic performance in 25 consecutive surgical patients. Relevant morphological variables in AAOCA were assessed by three independent blinded readers, with surgery as the reference standard. We used Cohen kappa coefficients and accuracies to assess agreement between readers and surgical findings, and we calculated intraclass correlation coefficients to compare length of the intramural course.

Results CT angiography correctly identified AAOCA in all patients. For the three readers, accuracies for detecting ostial stenosis were 84%, 94% and 96%; for high ostial origin, accuracies were 76%, 78% 82%; for intramurality using the peri-coronary fat sign, accuracies were 98%, 96% and 92%; and for intramurality using oval shape of coronary artery, accuracies were 98%, 94% and 92%. The intraclass correlation coefficients (ICCs) for predicting intramural length among the three readers were 0.67, 0.75 and 0.81 using peri-coronary fat, and 0.69, 0.50 and 0.81 using oval shape, respectively.

Conclusion CT angiography reliably identified AAOCA in all children and detected the presence of intramurality with high accuracy.

Keywords Anomaly · Children · Computed tomography angiography · Congenital heart disease · Coronary artery · Heart · Sudden cardiac death

✉ Rajesh Krishnamurthy
Rajesh.Krishnamurthy@nationwidechildrens.org

[1] Department of Radiology,
Nationwide Children's Hospital,
The Ohio State University,
700 Children's Drive,
Columbus, OH 43205, USA

[2] Department of Pediatric Radiology,
Texas Children's Hospital,
Baylor College of Medicine,
Houston, TX, USA

[3] Coronary Anomalies Program,
The Lillie Frank Abercrombie Section of Cardiology,
Texas Children's Hospital,
Baylor College of Medicine,
Houston, TX, USA

[4] Department of Biostatistics and Data Science,
University of Texas Health Science Center School of Public Health,
Houston, TX, USA

[5] Pediatric Cardiology,
Pediatric & Congenital Cardiology Associates of Texas,
Austin, TX, USA

[6] Texas Center for Pediatric and Congenital Heart Disease,
University of Texas Dell Medical School/Dell Children's Medical Center,
Austin, TX, USA

Introduction

Anomalous aortic origin of a coronary artery (AAOCA) from the incorrect coronary sinus of Valsalva is considered to be the second leading cause of sudden cardiac death in young athletes in the United States [1]. Left main coronary artery originating from the right sinus of Valsalva (ALCA) and the right coronary artery arising from the left sinus of Valsalva (ARCA) represent the most common subtypes of AAOCA, with the former carrying at least a 20-fold higher risk of sudden death [2]. The true prevalence of AAOCA is unknown. A recent study by Angelini and colleagues using cardiac MRI in a cohort of asymptomatic middle-school children found the prevalence of AAOCA to be as high as 0.7% [3]. Therefore it might be only a minority of children who come to clinical attention because of symptoms such as chest pain, palpitations, pre-syncope or syncope at rest or with exertion. The exact pathophysiological mechanism leading to ischemia and sudden cardiac death in children with AAOCA has not been elucidated. Potential morphological triggers for myocardial ischemia include an acute angle of takeoff of the anomalous coronary artery from the aortic wall creating a slit-like ostium that collapses or compresses easily, intrinsic stenosis of the ostium, hypoplasia of the proximal course, and an intramural segment of the proximal coronary artery that might be compressed within the aortic wall, or between the aorta and pulmonary artery [4, 5]. A high origin of the coronary artery might also predispose children to ischemia by removing the effect of the aortic sinus on coronary flow in diastole. Based on this understanding, certain anatomical and morphological characteristics including interarterial course (coronary artery traveling between the aorta and pulmonary trunk), intramural course (a segment of the anomalous coronary artery contained in the wall of the aorta), slit-like ostium, and ostial stenosis have been suggested as high-risk morphology for sudden cardiac death in children with origin of coronary arteries from contralateral sinus [5–7]. These anatomical substrates offer potential targets for risk stratification of children into high-risk and low-risk groups using noninvasive imaging and functional testing.

There is controversy about the best treatment options for children with AAOCA. Based on American College of Cardiology and American Heart Association guidelines, surgical intervention is indicated for ALCA with interarterial course, and for symptomatic patients with ARCA [8]. Some programs believe that asymptomatic patients with ARCA who have high-risk anatomical features (i.e. intramural course of proximal coronary artery, slit-like ostium and high origin of the coronary artery) might benefit from surgical intervention [9]. Therefore, a noninvasive technique like CT angiography that can be used to detect this anomaly and depict the high-risk anatomical characteristics accurately would have a significant role in determining management [10].

As part of the diagnostic workup, cross-sectional imaging with echocardiography, MRI or CT is performed in almost all cases, along with functional testing for evidence of myocardial ischemia with a cardiopulmonary exercise test, and a nuclear/MR/echocardiographic stress perfusion scan. Coronary CT angiography has been considered the primary imaging modality for evaluating coronary artery anatomy in this setting [11, 12], and is already widely used for this purpose. A standardized approach to interpreting CT angiography in the setting of AAOCA is needed to stratify children based on morphological risk factors and to compare management strategies among institutions. The diagnostic accuracy of CT angiography for detecting individual risk factors in the setting of AAOCA must also be established to help guide decisions on risk stratification and management.

We performed this study to determine the diagnostic accuracy of retrospective electrocardiogram (ECG)-gated CT angiography with structured interpretation for morphological characteristics that might determine risk in children with anomalous aortic origin of the coronary artery by comparing them to surgical findings.

Materials and methods

This prospective study was approved by our institutional review board and complied with the Health Insurance Portability and Accountability Act. We obtained written informed consent from all participants.

Study population

Children referred to our coronary anomalies program with suspected AAOCA underwent diagnostic workup and management according to a uniform algorithm (Online Supplementary Material 1). Every child referred to the program for suspicion of AAOCA underwent standardized evaluation, which included retrospective ECG-gated volumetric CT angiography with a 320-detector scanner. The clinical information, imaging studies and surgical data of all patients were entered into a longitudinal database. In this study, we retrospectively reviewed data from consecutive children and adolescents who were evaluated by the multidisciplinary team in 2014–2015 and underwent surgical intervention during the initial experience. The indications for surgery and surgical outcomes have been published [13] and there is no overlap with the imaging focus of this study.

Computed tomography angiography protocol

Electrocardiogram-gated studies were performed using a volumetric technique with a 320-detector scanner (Aquilion

ONE; Canon Medical Systems, Ōtawara, Japan). Studies were obtained without sedation or beta-blockade, and during volitional breath-holding where possible. Our system did not retain the records for heart rate at the time of the CT. Based on the recollection of the authors, the heart rates were typical for the patient's age, ranging 70–100 beats per minute (bpm). The gantry rotation time was 0.35 s. Tube voltage was set at 80–120 kV, and tube current at 150–400 mA based on the patient's age and weight. About 1.5–2.0 mL/kg of the nonionic contrast agent Optiray 320 mg/mL (Mallinckrodt Medical Inc., St. Louis, MO) was injected at a rate of 3–5 mL/s into a lower extremity peripheral vein via a 18- to 22-gauge (G) cannula. All images were obtained with retrospective ECG gating, with half-scan reconstruction used to reconstruct 20 phases at every 5% across the cardiac cycle. A three-dimensional adaptive iterative dose reduction algorithm (Toshiba Medical Systems, Ōtawara, Japan) was used to obtain 0.5-mm-thick axial slices. The PhaseXact scanner software (Toshiba Medical Systems) was used to automatically determine the cardiac phase with least cardiac motion for CT angiography image reconstruction. If a motion-free phase was not identified, image reconstruction proceeded to 1% intervals around the 5% intervals to identify artifact-free images of the coronary artery origins and proximal course.

Image analysis and standardized interpretation template

The Digital Imaging and Communications in Medicine (DICOM) datasets of pre-selected coronary CT angiography datasets were transferred to a post-processing workstation (Vitrea; Canon Medical Systems, Tustin, CA). Image-reformatting techniques, including multiplanar reformation, maximum-intensity projection and virtual angioscopy, were used for analysis of coronary CT angiography examinations. Oblique reformats were generated in the oblique axial, oblique coronal and oblique sagittal planes, which were parallel and orthogonal to the long-axis plane of the intramural course of the anomalous coronary artery. We generated virtual angioscopic images with a CT thresholding technique, which has been described [14], to produce intraluminal views of the right and left coronary artery ostia that simulated the appearance at surgery (Fig. 1). Three pediatric radiologists with 12 years (reader 2, R.K.), 7 years (reader 3, P.M.M.) and 3 years (reader 1, S.P.J.) of experience in pediatric cardiovascular imaging, who were blinded to the surgical findings and clinical information of patients, independently reviewed the 25 coronary CT angiography examinations using a standardized interpretation template. All morphological features were evaluated similarly at the time of surgery using the same reference standard template.

Reporting template

We synthesized the information from the variables to create a structured reporting template for AAOCA, which can be used for CT or MRI, and with minimal modification for echocardiography, catheter angiography and surgery (Fig. 2). The template contains coded numerical variables for the type of AAOCA, ostial morphology, location of the coronary ostia, ostial relationship, presence of intramural course, length of intramural course, coronary dominance, and presence of other abnormalities like intramyocardial course of the coronary artery or abnormal branching pattern.

The standardized CT angiography interpretation template contained the following variables for each coronary artery:

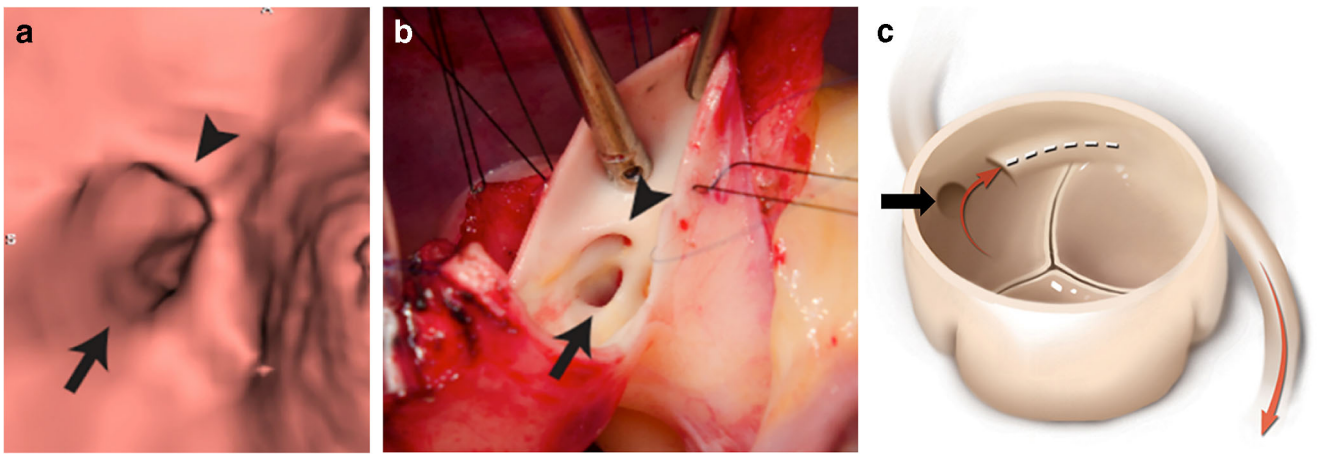

Fig. 1 Appearance of anomalous left coronary artery in an 8-year-old girl. **a** Virtual angioscopy. **b** Surgical photograph. **c** Artistic representation of the coronary ostia. Virtual angioscopy (**a**) and representative findings at surgery (**b**) show similarities in the coronary artery ostial appearance. Note the slit-like appearance of the left coronary artery ostium (*arrowhead*). The right coronary artery ostium (*arrow*) has a normal configuration. In (**c**), note the slit-like ostium and intramural course of the left coronary artery (*red arrows* and *dotted line*) and the normal rounded configuration of the right coronary artery (*black arrow*)

Reporting Template for Anomalous Aortic Origin of the Coronary Artery

1. Type of anomalous coronary
   - Right
   - Left
   - Both
2. Ostial location of RCA
   - 1, 2, 3 (sinus of origin)
   - a, b, c, X, Y, Z (radial location)
   - I, II, III, IV (vertical location)
3. Ostial location of LCA
   - 1, 2, 3 (sinus of origin)
   - a, b, c, X, Y, Z (radial location)
   - I, II, III, IV (vertical location)
4. Coronary dominance
   - Right/Left/Codominant
5. Ostial Relationship
   - 1 (separate coronary ostia)
   - 2 (adjacent coronary ostia)
   - 3 (single coronary ostium branching within the wall)
   - 4 (single coronary ostium branching outside the wall)
6. Ostial Morphology of anomalous coronary artery
   - Round
   - Oval
   - Slit-like
   - Pinhole
7. Intramural Course of anomalous coronary artery
   - Yes
   - No
8. Length of Intramural Course
   - -------- mm
9. Length of interarterial course
   - --------- mm
10. Other:
    - Course through thickened intercoronary pillar: Yes/No
    - Dynamic narrowing of coronary across cardiac cycle: Yes/No

Fig. 2 Reporting template for anomalous aortic origin of the coronary arteries (AAOCA). A slightly modified version of this template could be used to document key reporting elements in AAOCA for CT, MRI, echocardiography, catheter angiography and surgery. *LCA* left coronary artery, *RCA* right coronary artery

- *Type of AAOCA:* We classified the anomalous coronary artery as one of the following: (1) right coronary artery arising from left sinus, (2) left coronary artery arising from right sinus or (3) single coronary artery arising from the right or left sinus.
- *Location of coronary ostia:* We defined the exact location of the coronary ostia within the aorta using an alphanumeric coding system based on a standardized topography map (Fig. 3) that has been described [9]. The sinuses were labeled as 1, 2 or 3 starting with the right sinus, with a clockwise progression. The commissural locations were labeled as X, Y or Z starting with the right–left commissure. The middle 50% of a sinus was labeled as *b*, while the ipsilateral juxtacommissural regions were labeled as *a* and *c*, respectively. The vertical location of the coronary ostium was classified into four types according to the relationship to the level of the valve leaflet attachment to the aortic root and the sinotubular junction: (I) aortic annulus to commissural edge, (II) commissural edge to sinotubular junction, (III) at sinotubular junction, (IV) above the sinotubular junction. On CT angiography assessment, the dynamic three-dimensional (3-D) datasets were manipulated on the workstation with coronal cine imaging to distinguish level I (origin from the aortic root at or below the level of the valvular commissures, which are indicated by leaflet opening) from level II (origin from the aortic root above the level of the commissures and at the level of the column/pillar, which represent the suspensory support structures for the leaflet). Levels III and IV indicated a

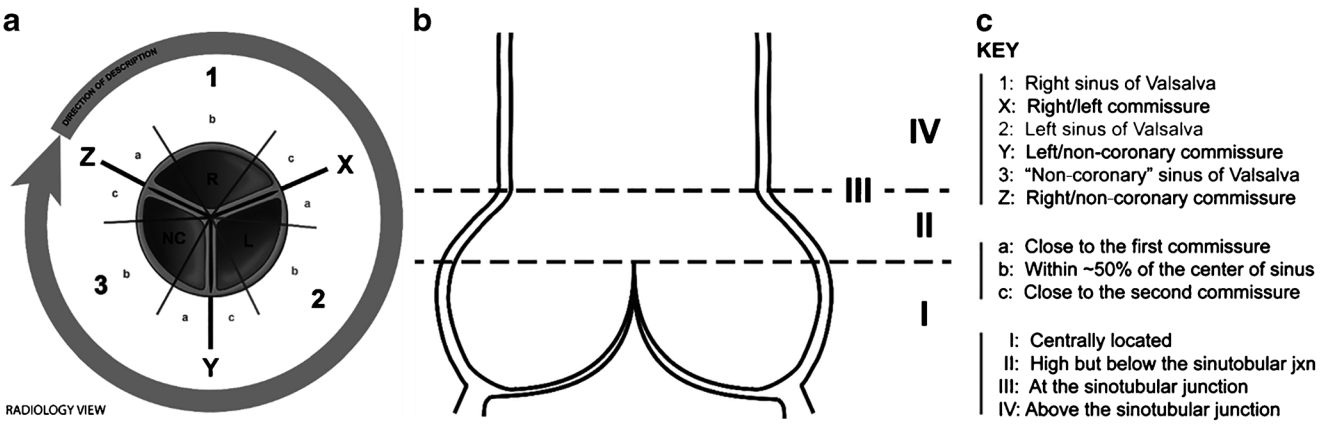

Fig. 3 Standardized nomenclature map used to describe the origin of the coronary arteries by CT, echocardiography or surgical findings. **a** Transverse view of the aortic root shows the radial location of the ostia, with *1*, *2* and *3* corresponding to the right, left and non-coronary sinuses, respectively. **b** Graphical representation of the coronal view of the aortic root and ascending aorta shows the vertical location of the ostia. **c** Key for the nomenclature on both views. Copyright 2013, Texas Children's Hospital (reprinted with permission)

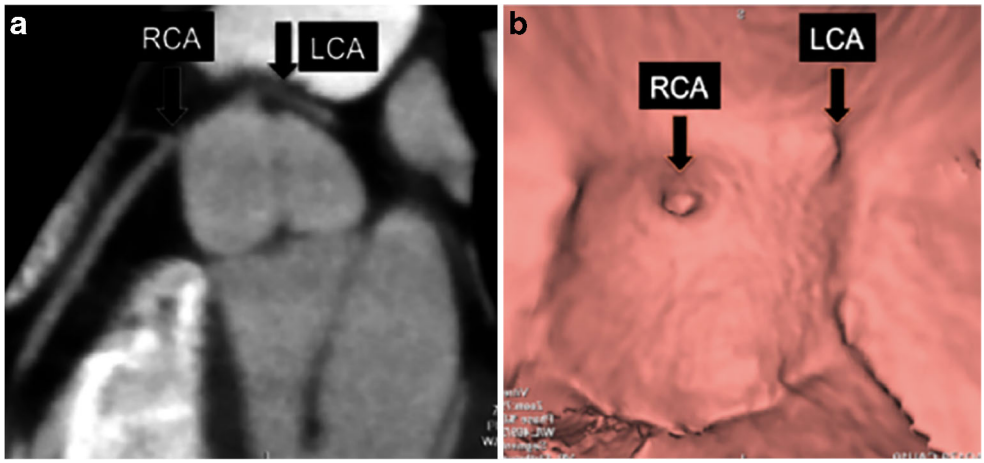

Fig. 4 Applying standardized nomenclature for ostial location in anomalous aortic origin of the coronary artery (AAOCA). **a** Coronal reformatted CT angiogram in a 16-year-old boy shows AAOCA of the left coronary artery (*LCA*) from the right sinus close to the right/left column, and at the level of the sinotubular junction (1c, level III) with an intramural course. The right coronary artery (*RCA*) ostium is located in the middle of the right sinus below the sinotubular junction (1b, II). **b** Corresponding virtual angioscopic image facing the ostia shows that the two ostia are separate from each other, corresponding to a type 1 ostial branching pattern

high location of the coronary ostium, at or above the sinotubular junction. An example of the use of CT to define location of the coronary ostia is given in Fig. 4.

- *Ostial relationship:* Relationships of the coronary ostia arising from the aortic root were classified as follows (Fig. 5):
  Type 1: separate ostia,
  Type 2: adjacent ostia,
  Type 3: single ostium branching within aortic wall, and
  Type 4: single ostium branching outside aortic wall (single coronary artery).
- *Ostial morphology:* The appearance of coronary ostium was classified as round, oval, slit-like or pinhole based on the appearance at virtual angioscopy (Fig. 6). The diagnosis of coronary artery ostial stenosis was made based on the presence of either a slit-like ostium or a pinhole ostium at virtual endoscopy. Severity of ostial stenosis was not graded.
- *Presence and length of intramural course:* The intramural course was defined as the course of the proximal coronary artery through the wall of the aorta prior to entering the mediastinum (Fig. 7). We used two independent methods to determine the presence and length of intramural segment of coronary artery by CT angiography:

  (1) Cross-sectional shape of the proximal coronary artery on multiplanar reformation: The intramural segment has an oval cross-sectional shape of lumen, while the mediastinal segment has a round shape.
  (2) Status of peri-coronary fat: The intramural segment has a thin wall of soft-tissue density on the luminal side, whereas the mediastinal segment has a complete peri-coronary cuff of low-density fat. We refer to the latter as the "peri-coronary fat sign" for intramurality. The calculation of intramural length using the peri-coronary fat sign and the coronary shape is illustrated in Fig. 7.

Surgical findings

Patients were offered surgical intervention based on the described algorithm (Online Supplementary Material 1), individual considerations and discussion with the family. Findings were recorded by the surgeon using the same standardized template as described for imaging. Type of AAOCA was determined by visual inspection. A coronary ostium was defined as slit-like if, on direct inspection, it appeared crescentic, with the superoinferior dimension being greater than the transverse one. The ostium was considered stenotic if the dimension of the ostium was qualitatively smaller than the dimension of the distal (non-intramural) coronary. Location of the ostia was recorded using the same topography map used for imaging.

To determine intramurality, the aortic root was completely dissected prior to arresting the heart, in particular around the area where the anomalous coronary arose from the aorta. After opening the aorta via an oblique aortotomy, the coronary artery was probed. A transmural fine stitch was placed from outside the aorta at the crotch of the anomalous coronary and into the aortic lumen. This stitch provided a sense of the length and direction of the intramural segment. After completely unroofing the intramural segment, a suture was used to measure the length of intramurality.

Statistical analysis

Statistical analysis was performed on SAS 9.3 software (SAS Institute, Cary, NC). To assess the agreement between each of

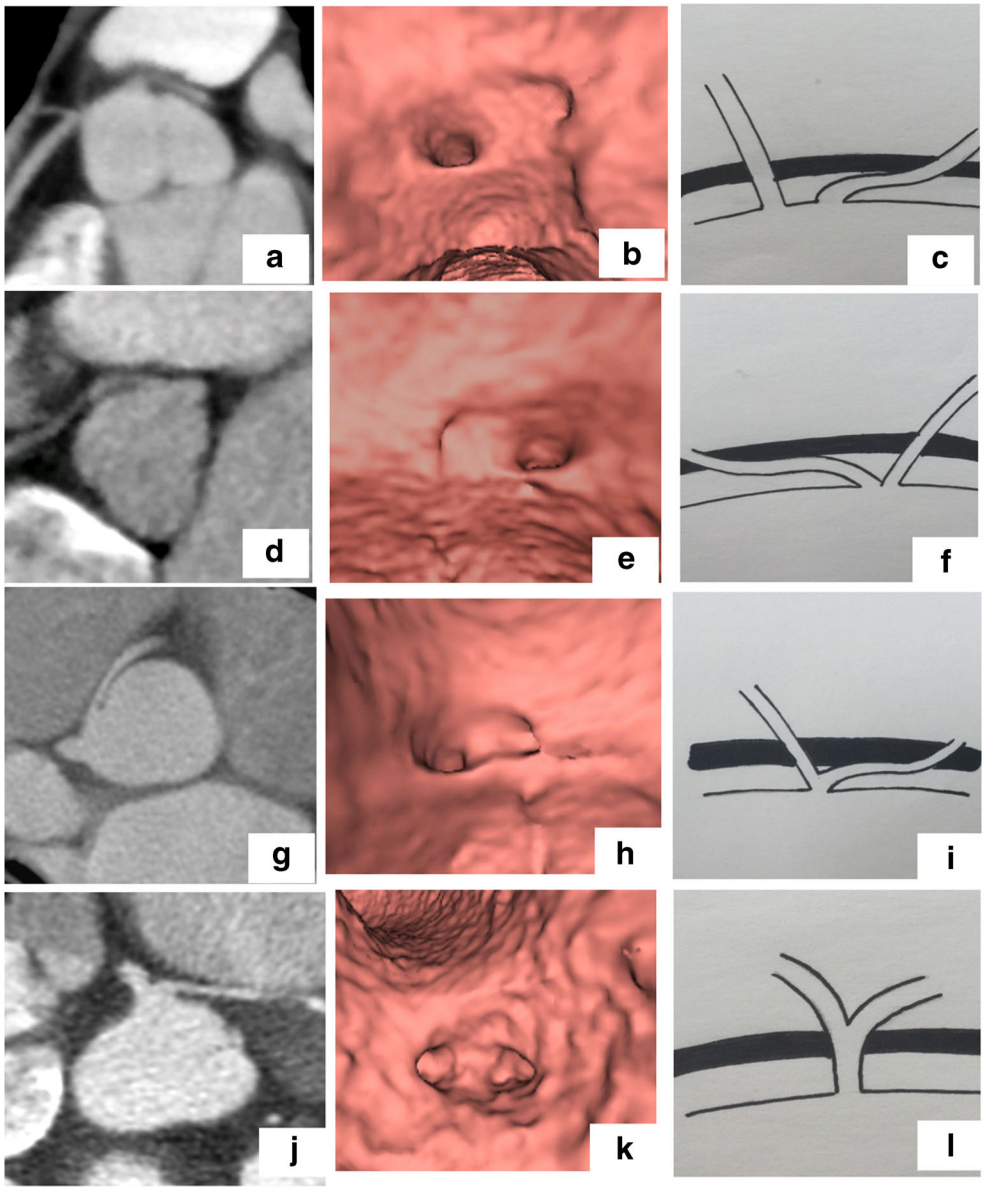

Fig. 5 Ostial branching pattern in anomalous aortic origin of the coronary artery (AAOCA). First column: cross-sectional multiplanar reformatted CT angiography images (**a**, **d**, **g** and **j**). Middle column: corresponding virtual angioscopic images of the coronary ostia (**b**, **e**, **h** and **k**). Last column: schematic of coronary ostial relationship types (**c**, **f**, **i** and **l**). Each row represents a type of ostial branching pattern seen in AAOCA. **a–c** Type 1 branching with separate ostia in a 16-year-old boy with anomalous left coronary artery with a slit-like ostium and an intramural course crossing the column. **d–f** Type 2 branching with adjacent ostia in a 10-year-old boy with anomalous right coronary artery with slit-like ostium and an intramural course. **g–i** Type 3 branching, with a single ostium bifurcating within the aortic wall in a 14-year-old boy. There is high origin of both coronary arteries above the sinotubular junction, with slit-like ostium of the left coronary artery and an intramural course. **j–l** Type 4 branching with a single ostium bifurcating outside the aortic wall in a 16-year-old boy. This represents a single coronary artery with round ostia of both coronary branches, without an intramural segment

the readers and the surgical findings, we calculated Cohen kappa coefficients and accuracies together with their 95% confidence intervals for categorical variables, and intraclass correlation coefficients (ICC) with 95% confidence intervals for the length of the intramural course. We created Bland–Altman scatter plots for length of intramurality for the three readers. We applied weighted kappa coefficients to variables with more than two ordered categories (i.e. radial location and ostial height), with higher weights when observations were farther apart. In addition, sensitivities, specificities, positive predictive values and negative predictive values were calculated for dichotomized variables. We calculated Fleiss kappa coefficients to estimate the agreement among the three readers for categorical variables. ICCs were calculated to estimate the agreement for continuous variables. To

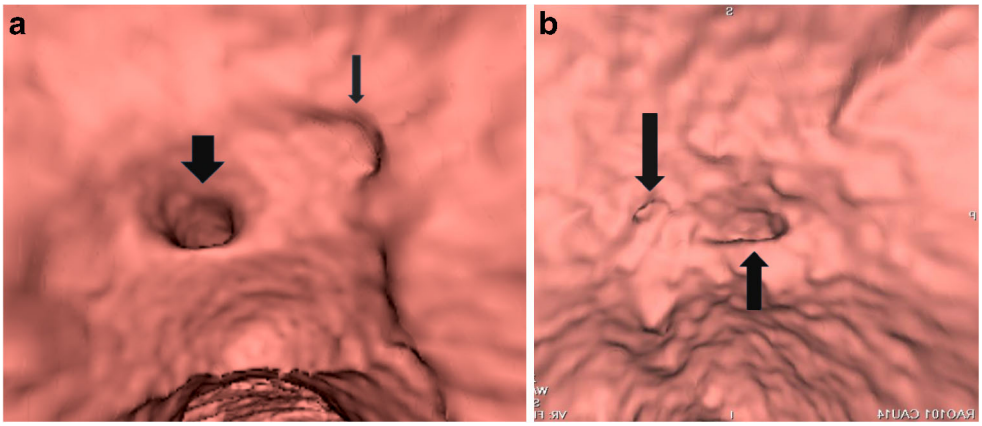

Fig. 6 Coronary ostial morphology. The coronary ostium is classified as round, oval, slit-like or pinhole based on a virtual angioscopic projection facing the ostium. **a** In a 12-year-old boy, the right coronary artery has a round orifice (*thick arrow*), while the anomalous left coronary artery has a slit-like orifice (*thin arrow*). **b** In a 9-year-old boy, the right coronary artery ostium (*down-facing arrow*) is pinhole in appearance, consistent with severe ostial stenosis. The left coronary artery ostium (*up-facing arrow*) is oval in shape. The ostia are adjacent to each other and located in the anterior aortic wall, just above the sinotubular junction

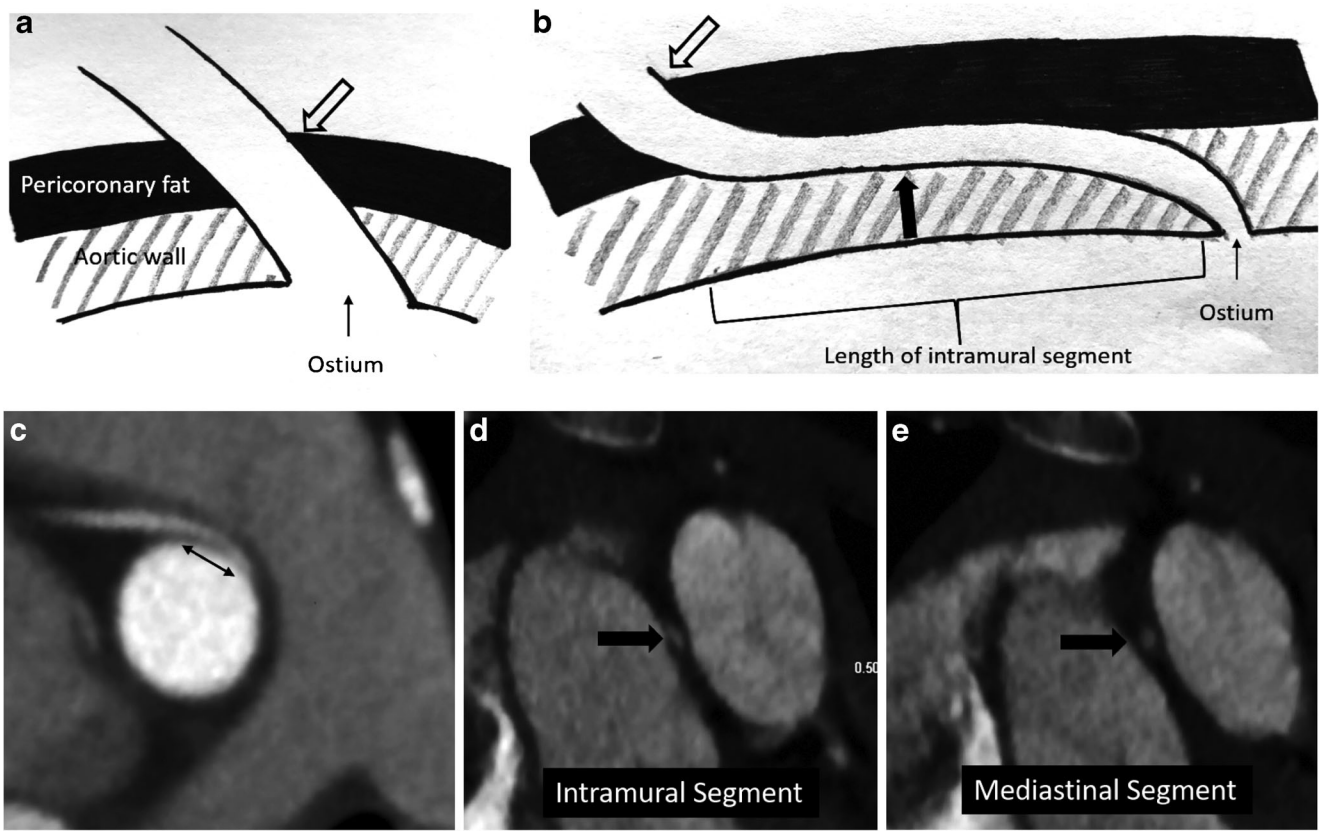

Fig. 7 Identification of intramurality on CT angiography. **a, b** Schematics show normal origin of the coronary artery (**a**) and intramural course of the coronary artery (**b**) to illustrate the peri-coronary fat sign. In the intramural segment, the black peri-coronary fat does not completely encase the coronary artery on the luminal aspect (*large solid arrow*), whereas in the mediastinum, the fat completely encases the coronary artery (*open arrow*). **c** Oblique reformatted long-axis CT image of an anomalous right coronary artery in a 14-year-old girl shows narrowing of the intramural segment (*line*) and an increase in caliber in the mediastinal segment. **d, e** Oblique sagittal CT images show the cross-section of the anomalous right coronary artery demonstrating the peri-coronary fat sign. The intramural segment has a thin wall of soft-tissue density on the luminal side (*arrow* in **d**) and an incomplete rim of low-density fat, whereas the mediastinal segment has complete peri-coronary cuff of dark fatty density, including on the luminal side (*arrow* in **e**). The cross-section of the intramural segment (**d**) also has an oval shape, as opposed to the round shape after it emerges from the aortic wall into the mediastinum (**e**)

interpret kappa and ICCs, we used the Cicchetti guidelines [15]: less than 0.40 — poor; between 0.40 and 0.59 — fair; between 0.60 and 0.74 — good; between 0.75 and 1.00 — excellent.

Results

Patient characteristics

A total of 25 consecutive children undergoing surgical intervention were assessed by this approach. The age of the study patients ranged from 4 months to 18 years at the time of surgery (median age: 12.5 years, interquartile range 5.1 years). The male-to-female ratio was 1.5:1.0. The mean volumetric CT dose index ($CTDI_{vol}$) was 17.3 mGy (range 9.3–24.3 mGy), mean dose–length product (DLP) was 280 mGy·cm (range 149–391 mGy·cm), and the mean calculated effective dose in mSv was 5.0 (range 2.7–7.0 mSv).

Type of anomalous aortic origin of the coronary artery

A total of 18 ARCA and 7 ALCA were found in 25 children and adolescents with CT angiography. The three readers showed complete agreement between CT angiography and surgery regarding the type of AAOCA (Table 1).

Location of coronary ostia

High origin of coronary artery was seen in 13/50 coronary arteries (26%). The diagnostic performance of CT angiography for detecting high take-off of coronary artery was 79% (Table 2). Kappa correlation coefficient (95% confidence intervals) for interobserver agreement for radial origin was 0.64 (0.51, 0.77) and for vertical origin was 0.25 (0.07, 0.44).

Coronary ostial relationship

There was complete agreement among the three readers between CT angiography and surgery regarding the relationship of the coronary ostia.

Ostial morphology

Among 50 coronary arteries directly assessed intraoperatively, 26 coronaries demonstrated oval or slit-like shape of the orifice. One child had abnormal appearance of both the right and left coronaries. Of the 26, 24 coronary arteries were classified as having a stenotic ostium. The diagnostic performance of CT angiography for detecting slit-like ostium and ostial stenosis is shown in Table 3. Kappa correlation coefficient (95% confidence intervals) for interobserver agreement for ostial stenosis was 0.75 (0.61, 0.90).

Presence of intramural course

Twenty-four patients had an intramural segment of the proximal portion of anomalous coronary artery identified at surgery. The presence of an oval cross-sectional shape of coronary artery on CT angiography had 98%, 94% and 92% accuracy for detecting surgically confirmed intramural segments. The diagnostic accuracy of CT angiography for detecting intramurality using the peri-coronary fat sign was similar (98%, 96% and 92%) (Table 4). Kappa correlation coefficient (95% confidence intervals) for interobserver agreement for intramural course based on peri-coronary fat was 0.92 (0.83, 1.00) and based on shape was also 0.92 (0.83, 1.00).

Length of intramural course

For the three readers, respectively, the intra-class correlation coefficients for predicting intramural length were 0.67, 0.75 and 0.81 using peri-coronary fat, and 0.69, 0.50 and 0.81 using oval shape (Table 5). Bland–Altman plots for the three readers for determining intramural length using the peri-coronary fat sign and the oval cross-sectional shape of the proximal coronaries are in Online Supplementary Material 2. Scatter plots with regression lines for length of intramurality based on peri-coronary fat and cross-sectional shape, compared with surgery, are provided in Fig. 8.

Discussion

The present study indicates that volumetric coronary CT angiography with retrospective ECG-gating, using a standardized interpretation template, allows for the accurate detection of the likely pathological substrates in various types of AAOCA when compared to surgery as the reference standard. Our results also indicate that the status of peri-coronary fat and the oval shape of the proximal coronary artery on CT represent reliable methods to delineate the presence and length of intramurality.

A structured CT angiography report that describes relevant pathological targets in AAOCA and is used along with functional testing in a multi-disciplinary setting to manage children with AAOCA might offer high clinical utility for therapeutic decision-making and allow surgical choices and results from different centers to be compared for the same anatomical risk factors. Standardized morphological features like location of the ostium, ostial branching pattern, the presence of ostial stenosis, and the presence and length of intramurality might be able to predict the type of surgery needed for an individual patient and should allow for better risk–benefit analysis because surgical risks vary with the type of procedure. For instance, the proximal course of the anomalous coronary artery with a level 1 or 2 origin would travel through the commissure or column, respectively, and surgical unroofing should consider the potential to

Table 1 Diagnostic performance of CT angiography for type of anomaly in 25 children and adolescents: right versus left

Variable	Surgery	Reader 1	Reader 2	Reader 3
Major anomaly (right)	18 (72%)	18 (72%)	18 (72%)	18 (72%)
Kappa (95% CI)		1 (1–1)	1 (1–1)	1 (1–1)
Accuracy with 95% CI		100 (78–100)	100 (78–100)	100 (78–100)
Major anomaly (left)	7 (28%)	7 (28%)	7 (28%)	7 (28%)
Kappa (95% CI)		1 (1–1)	1 (1–1)	1 (1–1)
Accuracy with 95% CI		100 (56–100)	100 (56–100)	100 (56–100)

CI confidence interval

destabilize the suspensory apparatus of the leaflets resulting in aortic regurgitation, with coronary translocation being an alternative surgical option. The impact of such a standardized diagnostic approach to risk stratification and surgical decision-making can be investigated in future work.

Electrocardiogram-gated coronary CT angiography is an accepted modality of choice for detecting coronary artery abnormalities [16]. One study showed that coronary CT angiography could determine with high accuracy the presence or absence of an intramural segment using elliptical shape of the anomalous coronary ostium [17]. In this study, we examined the accuracy of CT angiography to determine the presence and length of the intramural segment by the oval shape of the proximal coronary artery as well as a new peri-coronary fat sign. A recent multi-institutional study reported that symptomatic patients with anomalous coronary artery had a longer intramural course than asymptomatic patients [5]. Therefore, reliable identification of intramural length is an important part of diagnostic evaluation. The current reference standard for identifying intramural length is intravascular US, which is limited by its invasive nature and the lack of widespread expertise in the setting of AAOCA. The availability of two independent signs, namely the oval shape and the absence of the peri-coronary cuff of fat, for identifying and assessing length of intramurality on CT enhances the diagnostic confidence of CT in this setting. The incremental value of availability of a second sign for intramurality in addition to the widely used oval shape needs to be studied in a larger series.

Our study showed overall high accuracy of these signs among readers of varying experience for detecting intramurality. But it also showed that interobserver agreement varied depending on the morphological attribute. It was excellent for identifying the type of anomalous coronary artery, ostial stenosis, ostial relationship, and presence of intramural and interarterial course, good to excellent for intramural length and radial location of the ostium, fair for vertical location of the ostium, and poor for course through the commissure or inter-coronary pillar. The poor performance in identifying a high origin of the coronary artery above the sinotubular junction was a result of disagreement between the readers on where the sinotubular junction, essentially a discrete line, was located. Because the ostium is commonly located at the sinotubular junction, there was disagreement on whether the vertical level was II, III or IV. It is unclear whether this is clinically relevant because all clear-cut cases of high origin well above the sinotubular junction were accurately identified. We recommend that vertical levels III and IV be combined into a single category because they represent abnormally high origin of the coronary artery, where the coronary does not benefit from the pooling of blood in the sinus that promotes filling in diastole. The poor performance with respect to course through the intercoronary column was also a result of the frequent location of the proximal course of the anomalous coronary artery at the sinotubular junction, resulting in disagreement on whether it touched the top of the column or passed just superior to the column. The column

Table 2 Diagnostic performance of CT angiography for ostial location

Variable	Surgery	Reader 1	Reader 2	Reader 3
Radial location of ostium (*n*=50 cor)				
Weighted kappa (95% CI)		0.8 (0.7–0.9)	0.8 (0.7–1)	0.8 (0.7–0.9)
Height of ostium (*n*=50 cor)	13 (26%)	19 (38%)	14 (28%)	2 (4%)
Kappa (95% CI)		0.5 (0.2–0.7)	0.5 (0.3–0.8)	0.2 (0–0.5)
Accuracy % (95% CI)		76 (62–86)	82 (68–91)	78 (64–88)
Sensitivity % (95% CI)		77 (46–95)	69 (39–91)	15 (2–45)
Specificity % (95% CI)		76 (59–88)	86 (71–95)	100 (91–100)
PPV % (95% CI)		53 (29–76)	64 (35–87)	100 (16–100)
NPV % (95% CI)		90 (74–98)	89 (74–97)	77 (63–88)

CI confidence interval, *cor* coronaries, *NPV* negative predictive value, *PPV* positive predictive value

Table 3 Diagnostic performance of CT angiography for ostial morphology

Variable	Surgery	Reader 1	Reader 2	Reader 3
Slit-like ostium (*n*=50 cor)	26 (52%)	18 (36%)	24 (48%)	25 (50%)
Kappa (95% CI)		0.7 (0.5–0.9)	0.9 (0.8–1)	0.9 (0.7–1)
Accuracy % (95% CI)		84 (70–92)	96 (85–99)	94 (82–98)
Sensitivity % (95% CI)		69 (48–86)	92 (75–99)	92 (75–99)
Specificity % (95% CI)		100 (86–100)	100 (86–100)	96 (79–100)
PPV % (95% CI)		100 (81–100)	100 (86–100)	96 (80–100)
NPV % (95% CI)		75 (57–89)	92 (75–99)	92 (74–99)
Ostial stenosis (*n*=50 cor)	24 (48%)	16 (32%)	22 (44%)	23 (46%)
Kappa (95% CI)		0.7 (0.5–0.9)	0.9 (0.8–1.0)	0.9 (0.7–1.0)
Accuracy % (95% CI)		84 (70–92)	96 (85–99)	96 (85–99)
Sensitivity % (95% CI)		67 (45–84)	92 (73–99)	92 (73–99)
Specificity % (95% CI)		100 (87–100)	100 (87–100)	96 (80–100)
PPV % (95% CI)		100 (79–100)	100 (85–100)	96 (78–100)
NPV % (95% CI)		76 (59–89)	93 (77–99)	93 (76–99)

CI confidence interval, *cor* coronaries, *NPV* negative predictive value, *PPV* positive predictive value

was identified by a small wedge-shape area of soft tissue projecting into the lumen, but this became progressively harder to see as the column thinned toward the sinotubular junction. One reader (reader 3) consistently under-called high origin as well as course through the column in this study. From a surgical standpoint, almost all cases of levels III or IV origin with proximal intramural course touching the top of the column would be candidates for unroofing without the need for resuspension of the aortic valve leaflet. On the other hand, level II origin with course through the column would typically require either taking down the valve leaflet with resuspension during unroofing, or a coronary translocation to preserve integrity of valve function and avoid postoperative aortic regurgitation.

Although the volumetric CT technique used in this study significantly reduced the radiation exposure when compared to 64-detector technology, optimal imaging of coronary arteries, particularly in free-breathing pediatric patients with high heart rates, requires acquisition of isotropic data with high temporal and spatial resolution, which limits the implementation of certain radiation-dose-reduction techniques such as prospective ECG gating [18, 19]. Retrospective ECG-gating technique used in this protocol is considered the best method to reliably obtain motion-free

Table 4 Diagnostic performance of CT angiography for presence of intramurality (IM)

Variable	Surgery	Reader 1	Reader 2	Reader 3
Presence of IM by peri-coronary fat (*n*=50 cor)	24 (48%)	23 (46%)	24 (48%)	26 (52%)
Kappa (95% CI)		1 (0.9–1)	0.9 (0.8–1)	0.8 (0.6–0.9)
Accuracy % (95% CI)		98 (88–100)	96 (85–99)	92 (80–97)
Sensitivity % (95% CI)		96 (79–100)	96 (79–100)	96 (79–100)
Specificity % (95% CI)		100 (87–100)	96 (80–100)	88 (71–98)
PPV % (95% CI)		100 (85–100)	96 (79–100)	88 (70–98)
NPV % (95% CI)		96 (81–100)	96 (80–100)	96 (80–100)
Presence of IM by oval shape (*n*=50 cor)	24 (48%)	23 (46%)	25 (50%)	26 (52%)
Kappa (95% CI)		1 (0.9–1)	0.9 (0.7–1.0)	0.8 (0.6–0.9)
Accuracy % (95% CI)		98 (88–100)	94 (82–98)	92 (80–97)
Sensitivity % (95% CI)		96 (79–100)	96 (79–100)	96 (79–100)
Specificity % (95% CI)		100 (87–100)	92 (76–99)	88 (71–98)
PPV % (95% CI)		100 (85–100)	92 (74–99)	88 (70–98)
NPV % (95% CI)		96 (81–100)	96 (80–100)	96 (80–100)

CI confidence interval, *cor* coronaries, *NPV* negative predictive value, *PPV* positive predictive value

Table 5 Diagnostic performance of CT angiography for length of intramurality (IM)

Variable	Surgery	Reader 1	Reader 2	Reader 3
IM length by fat (mm) (*n*=25 cor)[a]	6 (0–9)	5 (0–11)	5.4 (1–11)	4.7 (1.6–9.8)
ICC (95% CI)		0.67 (0.43, 0.84)	0.75 (0.54, 0.88)	0.81 (0.64, 0.91)
IM length by shape (mm) (*n*=25 cor)[a]	6 (0–9)	5.75 (0–11)	5.7 (2–104)	4.8 (1.8–11.1)
ICC (95% CI)		0.69 (0.46, 0.85)	0.50 (0.23, 0.76)	0.81 (0.64, 0.91)

CI confidence interval, *cor* coronaries, *ICC* intraclass correlation coefficient

[a] Only included coronaries that were deemed to be major anomalies

coronary images across the cardiac cycle for assessing dynamic narrowing. There is a growing interest in cardiac MRI for assessing the coronary arteries [20–22]. A recent study in a small group of patients with low heart rate and regular breathing pattern showed that coronary MR angiography could accurately determine the presence or absence of an intramural segment in an anomalous coronary artery [22]. However, MR angiography is not widely used for assessing coronary arteries because of its relatively high failure rate in children with higher heart rates, and its inability to match CT angiography in providing dynamic coronary imaging with high spatial resolution across the cardiac cycle. These limitations are expected to improve with recent advances in cardiac MRI like blood pool contrast agents [23], and the structured interpretation approach described in this paper should be valid for MR interpretations as well.

Our study had some limitations. One, because AAOCA is a relatively rare congenital malformation, the number of patients in our study is small. However, it represents the largest continuous series of AAOCA children and adolescents undergoing standardized imaging assessment and corresponding surgical data collection. Two, our study population consisted of symptomatic high-risk patients who underwent surgical intervention, resulting in a bias in patient selection that might have led to overestimation of the diagnostic performance. But comparison of individual morphological features between imaging and surgery is still valid. Three, the use of the peri-coronary fat sign is dependent on adequate image quality that allows distinction between soft tissue and fat. We have anecdotally encountered patients who had very little mediastinal fat or had excessive image noise that prevented this assessment, although none was encountered in this study. The oval shape can still be used as a reliable sign of intramurality in these patients. Four, the measurements and observations made on CT angiography might vary minimally with the phase of the cardiac cycle. This was not assessed on this study. The best phase was chosen based on qualitative assessment of motion and was used for diagnostic assessment. Dynamic changes in morphology and caliber of the proximal course of the anomalous coronary artery were not studied.

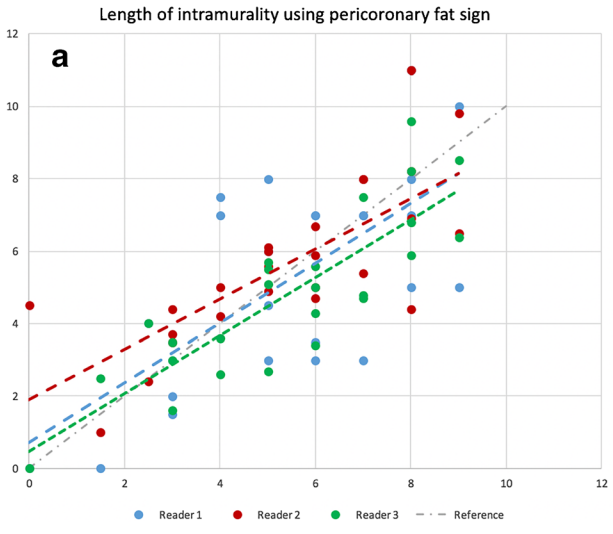

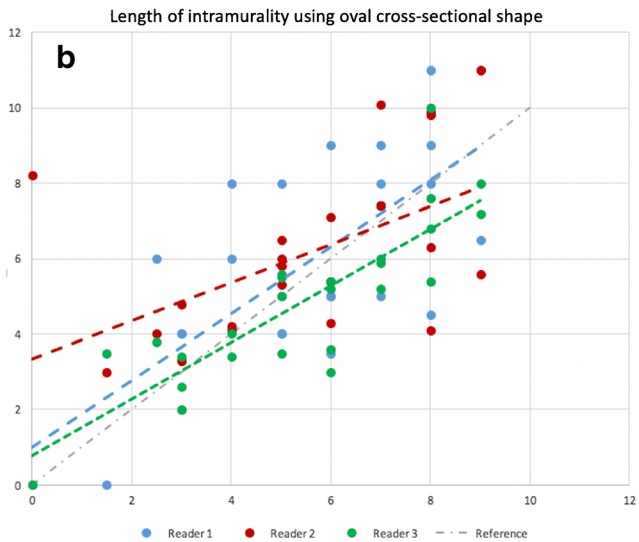

Fig. 8 Performance of the three readers for determining length of intramurality. **a** Peri-coronary fat sign. Scatter plots with regression lines for length of intramurality using the peri-coronary fat sign on CT angiography for three readers compared with findings at surgery as the reference standard. **b** Oval cross-sectional shape. Scatter plots with regression lines for length of intramurality using an oval cross-sectional shape of the coronary artery on CT angiography for three readers compared with findings at surgery as the reference standard

Conclusion

CT angiography reliably identified AAOCA in all patients, detected ostial stenosis and ostial location with moderate accuracy, and detected the presence of intramurality with high accuracy. A standardized CT angiography protocol combined with a structured reporting template that describes high-risk morphology in AAOCA, and is used along with functional testing, might be useful for risk stratification and treatment planning.

Supplementary Information The online version contains supplementary material available at https://doi.org/10.1007/s00247-021-05011-0.

Declarations

Conflicts of interest None

References

1. Maron BJ, Doerer JJ, Haas TS et al (2009) Sudden deaths in young competitive athletes: analysis of 1,866 deaths in the United States, 1980-2006. Circulation 119:1085–1092
2. Basso C, Maron BJ, Corrado D, Thiene G (2000) Clinical profile of congenital coronary artery anomalies with origin from the wrong aortic sinus leading to sudden death in young competitive athletes. J Am Coll Cardiol 35:1493–1501
3. Angelini P (2014) Novel imaging of coronary artery anomalies to assess their prevalence, the causes of clinical symptoms, and the risk of sudden cardiac death. Circ Cardiovasc Imaging 7:747–754
4. Taylor AJ, Byers JP, Cheitlin MD, Virmani R (1997) Anomalous right or left coronary artery from the contralateral coronary sinus: "high-risk" abnormalities in the initial coronary artery course and heterogeneous clinical outcomes. Am Heart J 133:428–435
5. Jegatheeswaran A, Devlin PJ, McCrindle BW et al (2019) Features associated with myocardial ischemia in anomalous aortic origin of a coronary artery: a Congenital Heart Surgeons' Society study. J Thorac Cardiovasc Surg 158:822–834.e3
6. Frescura C, Basso C, Thiene G et al (1998) Anomalous origin of coronary arteries and risk of sudden death: a study based on an autopsy population of congenital heart disease. Hum Pathol 29: 689–695
7. Eckart RE, Scoville SL, Campbell CL et al (2004) Sudden death in young adults: a 25-year review of autopsies in military recruits. Ann Intern Med 141:829–834
8. Warnes CA, Williams RG, Bashore TM et al (2008) ACC/AHA 2008 guidelines for the management of adults with congenital heart disease: a report of the American College of Cardiology/American Heart Association task force on practice guidelines (writing committee to develop guidelines on the management of adults with congenital heart disease). Developed in collaboration with the American Society of Echocardiography, Heart Rhythm Society, International Society for Adult Congenital Heart Disease, Society for Cardiovascular Angiography and Interventions, and Society of Thoracic Surgeons. J Am Coll Cardiol 52:e143–e263
9. Mery CM, Lawrence SM, Krishnamurthy R et al (2014) Anomalous aortic origin of a coronary artery: toward a standardized approach. Semin Thoracic Surg 26:110–122
10. Balasubramanya S, Mongé MC, Eltayeb OM et al (2017) Anomalous aortic origin of a coronary artery: symptoms do not correlate with intramural length or ostial diameter. World J Pediatr Congenit Heart Surg 8:445–452
11. Lederlin M, Thambo J-B, Latrabe V et al (2011) Coronary imaging techniques with emphasis on CT and MRI. Pediatr Radiol 41:1516–1525
12. Shriki JE, Shinbane JS, Rashid MA et al (2012) Identifying, characterizing, and classifying congenital anomalies of the coronary arteries. Radiographics 32:453–468
13. Mery CM, De Leon LE, Molossi S et al (2018) Outcomes of surgical intervention for anomalous aortic origin of a coronary artery: a large contemporary prospective cohort study. J Thorac Cardiovasc Surg 155:305–319
14. Sun Z, Dimpudus FJ, Nugroho J, Adipranoto JD (2010) CT virtual intravascular endoscopy assessment of coronary artery plaques: a preliminary study. Eur J Radiol 75:e112–e119
15. Cicchetti DV, Sparrow SA (1981) Developing criteria for establishing interrater reliability of specific items: applications to assessment of adaptive behavior. Am J Ment Defic 86:127–137
16. Girzadas M, Varga P, Dajani K (2009) A single-center experience of detecting coronary anomalies on 64-slice computed tomography. J Cardiovasc Med 10:842–847
17. Miller JA, Anavekar NS, Yaman El MM et al (2012) Computed tomographic angiography identification of intramural segments in anomalous coronary arteries with interarterial course. Int J Cardiovasc Imaging 28:1525–1532
18. Jadhav SP, Golriz F, Atweh LA et al (2015) CT angiography of neonates and infants: comparison of radiation dose and image quality of target mode prospectively ECG-gated 320-MDCT and ungated helical 64-MDCT. AJR Am J Roentgenol 204:W184–W191
19. Sun Z, Ng K-H (2012) Prospective versus retrospective ECG-gated multislice CT coronary angiography: a systematic review of radiation dose and diagnostic accuracy. Eur J Radiol 81:e94–e100
20. Clemente A, Del Borrello M, Greco P et al (2010) Anomalous origin of the coronary arteries in children: diagnostic role of three-dimensional coronary MR angiography. Clin Imaging 34:337–343
21. Beerbaum P, Sarikouch S, Laser K-T et al (2009) Coronary anomalies assessed by whole-heart isotropic 3D magnetic resonance imaging for cardiac morphology in congenital heart disease. J Magn Reson Imaging 29:320–327
22. Biko DM, Chung C, Hitt DM et al (2015) High-resolution coronary MR angiography for evaluation of patients with anomalous coronary arteries: visualization of the intramural segment. Pediatr Radiol 45:1146–1152
23. Han F, Rapacchi S, Khan S et al (2015) Four-dimensional, multiphase, steady-state imaging with contrast enhancement (MUSIC) in the heart: a feasibility study in children. Magn Reson Med 74: 1042–1049